machines

MDPI

Article

A Force Control Method Integrating Human Skills for Complex Surface Finishing

Kang Min, Fenglei Ni *, Zhaoyang Chen and Hong Liu

State Key Laboratory of Robotics and System, Harbin Institute of Technology, Harbin 150001, China
* Correspondence: flni@hit.edu.cn; Tel.: +86-186-0451-3569

Abstract: Force control is one of the core modules for surface finishing such as grinding, polishing and sanding. However, the current force control methods based on human skills lack in-depth analysis of data patterns or are only applicable to flat surfaces. In addition, surface finishing is mainly performed by hand, resulting in low processing efficiency and poor product consistency. Therefore, this paper proposes a force control method that incorporates human skills to achieve relatively accurate force skill transfer and complex surface finishing. Firstly, human skills consisting of the force skill and the motion skill are learned. The force skill is used to generate the desired force. Then, a series of discrete poses are obtained based on human demonstration and combined with the motion skill to generate the desired trajectory. Finally, a computed-torque impedance control method is proposed to achieve relatively accurate force skill transfer and complex surface finishing by incorporating the desired trajectory and the desired force. The experiments are conducted on a platform composed of a 7-DOF collaborative robot manipulator from Franka Emika and a complex violin surface. The results demonstrate that the proposed force control method can achieve relatively accurate force skill transfer and improve the surface quality of the workpiece.

Keywords: complex surface finishing; human skills learning; human demonstration; trajectory generation; impedance control

check for updates

Citation: Min, K.; Ni, F.; Chen, Z.; Liu, H. A Force Control Method Integrating Human Skills for Complex Surface Finishing. *Machines* **2024**, *12*, 756. https://doi.org/10.3390/machines12110756

Academic Editor: Gianni Campatelli

Received: 29 June 2024
Revised: 30 July 2024
Accepted: 3 August 2024
Published: 26 October 2024

Copyright: © 2024 by the authors. Licensee MDPI, Basel, Switzerland. This article is an open access article distributed under the terms and conditions of the Creative Commons Attribution (CC BY) license (https://creativecommons.org/licenses/by/4.0/).

1. Introduction

Surface finishing, such as grinding, polishing or sanding, is a crucial step in many manufacturing processes to achieve the desired properties of the workpiece surface [1]. Grinding is a manufacturing process that removes materials to shape the workpiece into the desired form [2]. In many cases, grinding is a cost-effective method for machining workpieces with complex surfaces and difficult-to-machine materials [3,4]. Polishing is an essential process in many precision manufacturing processes to remove surface imperfections and improve surface smoothness and brightness [5]. Sanding is an important procedure for manufacturing wood products and can be used to eliminate rough edges, surface imperfections or prepare for further finishing processes such as painting or staining [6]. Currently, surface finishing is mainly performed by hand, resulting in low processing efficiency and poor product consistency. In addition, the harsh working environment with high noise and dust has caused a shortage of skilled workers [7].

To solve the problems existing in manual work, many automated surface finishing methods have been proposed. For sanding, Nagata et al. [8] proposed a sanding system based on an industrial robot for the sanding of wooden furniture. In addition, the contact force between the sanding tool and the wooden workpiece was controlled to achieve the desired force tracking. Huo et al. [9] proposed an autonomous sanding robot and used structure light technology to model objects and assess their quality. In addition, an adaptive impedance controller was incorporated to control the sanding force. For grinding/polishing, robots are widely adopted because of the advantages of large workspace, low cost, and high flexibility [10]. Ma et al. [11] proposed a robot grinding path

planning method for complex surface workpieces based on B-spline curves and surfaces. Xiao et al. [12] proposed a robot polishing trajectory planning method for complex surfaces to achieve the desired material removal depth. Zhou et al. [13] proposed a framework based on the combination conditional dynamic movement primitives (CDMPs) with trajectory segmentation and node mapping methods to imitate robot grinding motion. Wang et al. [14] proposed a passive compliant control method to reduce force fluctuations in robot blade grinding. Chen et al. [15] proposed an active compliant force-controlled end-effector for the robot grinding of curved parts. Zhang et al. [16] proposed a hybrid force/position control to control the grinding force of aviation blades. Han et al. [17] proposed a nonlinear impedance control with trajectory adaptation for collaborative robot grinding. Although relevant studies are relatively rich, manual work remains predominant in the surface finishing of complex surfaces, especially those with unknown processing parameters. In addition, in the surface finishing of some workpieces composed of multiple complex surfaces, the complexity of the workpiece makes it impossible to achieve fully automated processing. Hence, it is very important to strengthen the cooperation between humans and robots [18].

Human-robot assisted surface finishing combines the dual advantages of humans and robots, providing a feasible method to solve these issues. Xie et al. [19] proposed a human-robot collaborative trajectory planning method for robotic belt grinding of complex surfaces. The experimental results show that this method can reduce the surface roughness of the workpiece and is superior to the skilled worker. Ng et al. [20–22] proposed a method to capture tacit knowledge of the grinding process. The material removal model based on key process variables (contact force, tool path, feedrate, etc.) was adopted to determine suitable parameters for robot grinding. In addition, the captured manual motions were used to optimize the robot machining path. Gao et al. [23] proposed a learning-based method to transfer force-related skills from human demonstrations to robots to achieve human-like manipulation. Polishing and assembly experiments demonstrated the effectiveness of the method. However, in the polishing experiment, the robot needed to move twice along the teaching trajectory to eliminate the force exerted by humans on the end-effector. Zhang et al. [24] proposed a method to transfer human skills to robot belt grinding. The human skills are encapsulated as a statistical model based on the Gaussian mixture model (GMM) and Gaussian mixture regression (GMR). The experiments demonstrated the effectiveness of the method. Ochoa et al. [25,26] proposed an impedance control method based on human skills for human-robot assisted mold polishing. The polishing experiments confirmed the effectiveness of the method. However, the method is limited to flat surface polishing. In addition, human skills are not well transferred to the robot.

In summary, the research on human-robot assisted surface finishing is still relatively scarce and mainly focuses on force skills, motion skills and processing techniques. Force control is one of the core modules for surface finishing. However, the current force control methods based on human skills lack in-depth analysis of data patterns or are only applicable to flat surfaces.

Therefore, this paper proposes a force control method that incorporates human skills to achieve relatively accurate force skill transfer and complex surface finishing. Furthermore, the proposed force control method is introduced by taking the sanding of a complex wooden surface as an example. The advantages are described as follows:

(1) Human skills are deeply analyzed and decomposed into motion skill and force skill. Thus, these human skills are easy to learn and transfer.
(2) A robot trajectory planning method based on spline curves is provided to generate the desired trajectory, meeting the requirements of complex surface trajectory planning.
(3) A computed-torque impedance control architecture considering null-space optimization is proposed for constant force tracking.

This paper is organized as follows: Section 2 presents an overview of the proposed method. Section 3 introduces the learning of human skills. Section 4 provides a trajectory planning method to generate the continuous desired trajectory. Section 5 presents an

impedance control scheme considering null-space optimization. Section 6 presents the experiment and results analysis. The conclusions are stated in Section 7.

2. Overview of the Algorithm

Manual work remains predominant in the finishing of complex surfaces, especially those with unknown processing parameters. Despite its many disadvantages, the expertise and experience of skilled workers remains an effective way to improve the quality of such workpieces.

Therefore, this paper proposes a force control method that integrates human skills to achieve relatively accurate force skill transfer and complex surface finishing. The method is implemented on a collaborative robot equipped with joint torque sensors to ensure safety. The method mainly consists of three parts: (1) human skills learning, (2) continuous desired trajectory generation and (3) impedance control considering null-space optimization. Furthermore, the proposed force control method is introduced by taking the sanding of the complex wooden surface as an example.

The sanding process based on the proposed force control method is illustrated in Figure 1. Firstly, human skills consisting of the force skill and the motion skill are learned. The force skill is used to generate the desired force. The motion skill mainly refers to the velocity and acceleration of the machining trajectory, which is related to the sanding force in the feed direction. Then, a series of discrete poses are obtained based on human demonstration and combined with the motion skill to generate the continuous desired trajectory. Finally, a computed-torque impedance control method considering null-space optimization is proposed. By incorporating the desired trajectory and the desired force, relatively accurate force skill transfer and sanding of the complex surface are achieved.

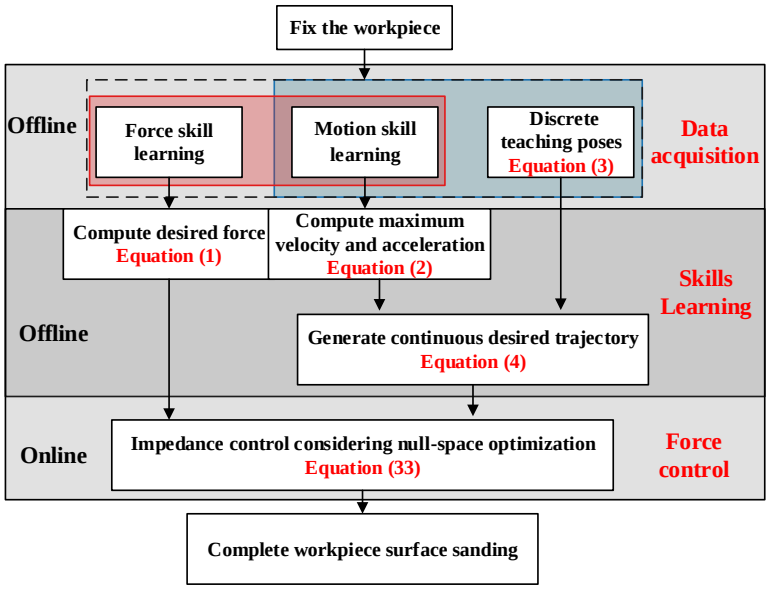

Figure 1. Sanding process based on the proposed force control method.

3. Human Skills Learning

The sanding force plays a crucial role in the surface quality and material removal rate of the workpiece. By analyzing the relative motion between the robot end pneumatic sanding tool and the workpiece, the sanding force can be decomposed into three orthogonal components, namely, normal sanding force, F_z; feed direction sanding force, F_y; and radial sanding force, F_x, as shown in Figure 2.

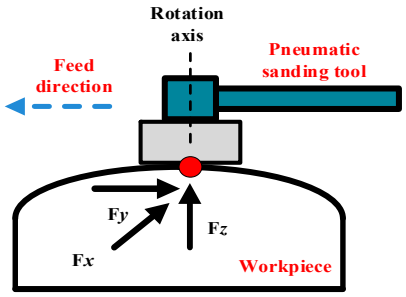

Figure 2. Schematic diagram of sanding forces on the complex surface.

F_x and F_y are mainly determined by F_z, the motion skill and processing parameters. The motion skill refers to the feed speed and acceleration of the machining trajectory. The processing parameters mainly refer to the rotation speed of the pneumatic sanding tool, the particle size of the sandpaper, etc. Therefore, it is necessary to learn both the motion skill and the force skill simultaneously to achieve relatively accurate force skill transfer when the processing parameters are fixed. In addition, in skill learning, the sampling period of force and position data is 1 ms.

3.1. Force Skill Learning

During force skill learning, the robot manipulator remains stationary to avoid the sanding force being partially absorbed by the human arm. The user grasps the workpiece to perform the sanding task and records the force data, as shown in Figure 3.

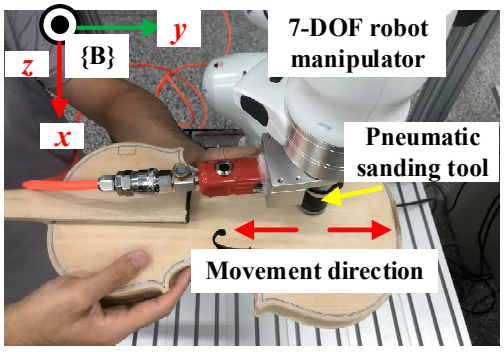

Figure 3. Force skill learning.

During sanding, the y-axis direction is the feed direction. In addition, the workpiece surface normal direction is adjusted in real time to ensure that it is consistent with the axial direction of the sanding tool. The recorded force data, excluding the sensor zero-drift values, are shown in Figure 4.

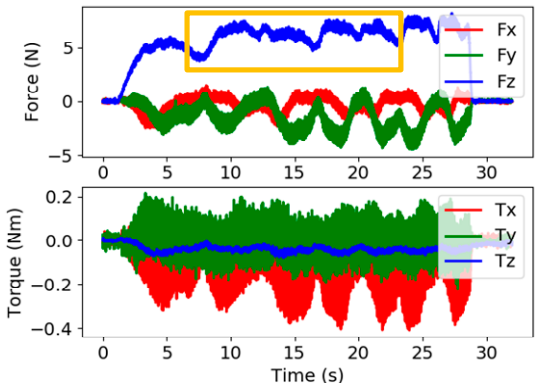

Figure 4. The force/torque values during sanding.

As shown in Figure 4, the surface sanding is mainly affected by the normal sanding force, F_z, and the feed direction sanding force, F_y. F_y is mainly determined by F_z and the motion skill. Assuming that F_z is approximately a constant, the force data recorded over a period of time were selected and their average value is computed:

$$F_z = 6.2\ \text{N} \tag{1}$$

Therefore, it is only necessary to maintain the normal contact force constant during sanding.

3.2. Motion Skill Learning

During motion skill learning, the user grasps the sanding tool under gravity compensation to move and records the position data, as shown in Figure 5.

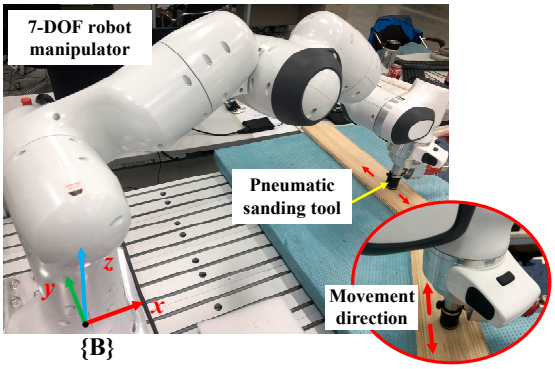

Figure 5. Motion skill learning.

During sanding, the axis of the sanding tool needs to be consistent with the workpiece surface normal direction. Thus, motion learning is performed on the horizontal plane because it is more efficient and suitable for human demonstration. The sanding tool moves back and forth mainly along the y-axis direction (or other directions) of the robot base. The recorded position data in three orthogonal directions are shown in Figure 6a.

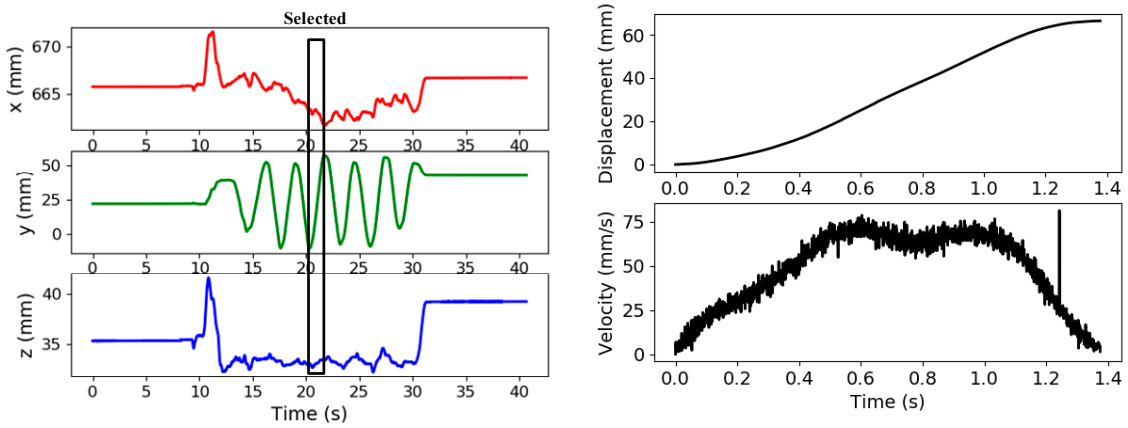

(**a**) (**b**)

Figure 6. The recorded position data and the displacement and velocity of the selected trajectory: (**a**) recorded position data; (**b**) displacement and velocity of the selected trajectory.

To better quantify the motion skill, a trajectory is randomly selected. Then, the displacement and velocity are calculated, as shown in Figure 6b. The displacement is obtained by sequentially adding the distances between two adjacent positions. The velocity is obtained by differencing the two adjacent displacements.

Based on the analysis, it can be concluded that the motion skill conforms to the T-shaped feedrate profile $s(t)$, including three stages: uniform acceleration $(0 - t_1)$, uniform velocity $(t_1 - t_2)$ and uniform deceleration $(t_2 - t_3)$, as shown in Figure 7.

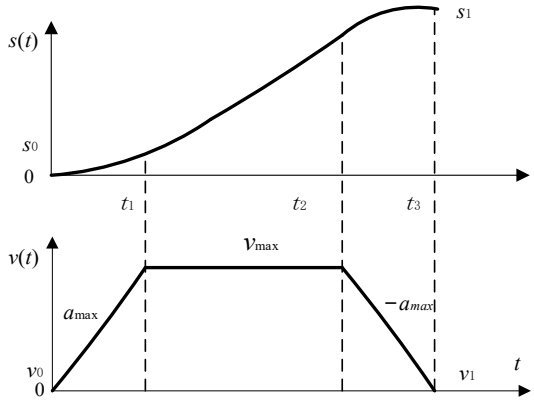

Figure 7. The T-shaped feedrate profile.

As shown in Figure 7, s_0 and v_0 are the displacement and velocity of the starting position, respectively. s_1 and v_1 are the displacement and velocity of the ending position, respectively. v_{max} and a_{max} are the maximum velocity and maximum acceleration, which compose the motion skill that needs to be learned. According to Figure 6b, the maximum velocity and maximum acceleration are computed as follows:

$$\begin{aligned} v_{max} &= 66.94 \text{ mm/s} \\ a_{max} &= 173.53 \text{ mm/s}^2 \end{aligned} \tag{2}$$

To verify the effectiveness of the motion skill learning, the selected trajectory is re-planned based on the learned maximum velocity and maximum acceleration, as shown in Figure 8.

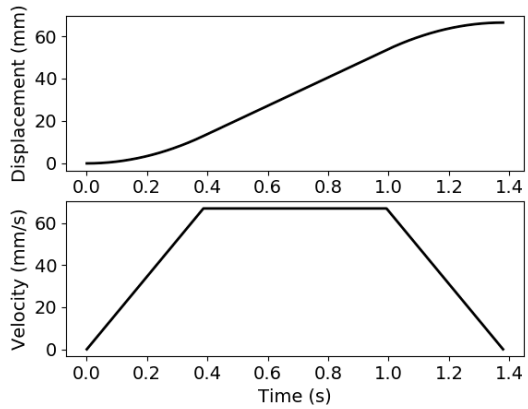

Figure 8. The re-planned displacement and velocity of the selected trajectory.

By comparing Figure 6b with Figure 8, it can be seen that the motion skill has been well learned. In the subsequent complex surface sanding, the transfer of the motion skill can be completed by applying the learned T-shaped feedrate profile to the determination of the trajectory motion law.

4. Continuous Desired Trajectory Generation

During sanding, the robot needs to ensure that the sanding tool moves along the workpiece surface. Thus, the user grasps the robot under gravity compensation to teach the discrete poses on the workpiece surface. Then, the continuous desired trajectory is generated based on the discrete poses and the learned T-shaped feedrate profile.

The discrete linear robot paths are acquired by coinciding the tool coordinate system (TCS) with the local coordinate system (LCS) of the workpiece. The LCS is established based on the position and its corresponding unit normal vector (z-axis direction) and the feed direction (y-axis direction), as shown in Figure 9.

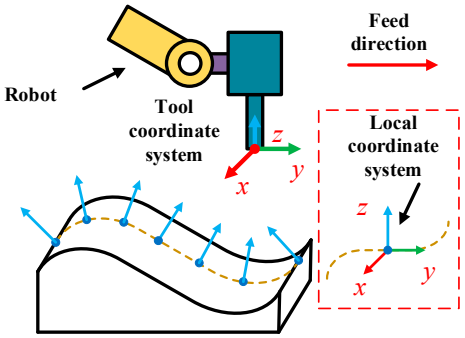

Figure 9. Schematic diagram of robot paths generation.

The transformation matrix, $\boldsymbol{T}$, of the tool coordinate system relative to the robot base coordinate system is denoted as follows:

$$\boldsymbol{T} = \begin{bmatrix} \boldsymbol{R} & \boldsymbol{P} \\ \boldsymbol{0} & 1 \end{bmatrix} \tag{3}$$

where $\boldsymbol{R} = \begin{bmatrix} r_{11} & r_{12} & r_{13} \\ r_{21} & r_{22} & r_{23} \\ r_{31} & r_{32} & r_{33} \end{bmatrix}, \boldsymbol{P} = \begin{bmatrix} x \\ y \\ z \end{bmatrix}$.

The positions can be directly fitted using the B-spline curve. Orientation fitting with the rotation matrix will destroy its orthogonality. Therefore, the rotation matrix is converted into the quaternion for orientation fitting.

Thus, the discrete teaching poses consist of a series of tool center positions, $\{\boldsymbol{p}_i\}_{i=0}^{n}$, and quaternion orientations, $\{\boldsymbol{q}_i\}_{i=0}^{n}$. Then, the desired trajectory is generated based on our previous work [27]. A flowchart of the trajectory planning method is shown in Figure 10.

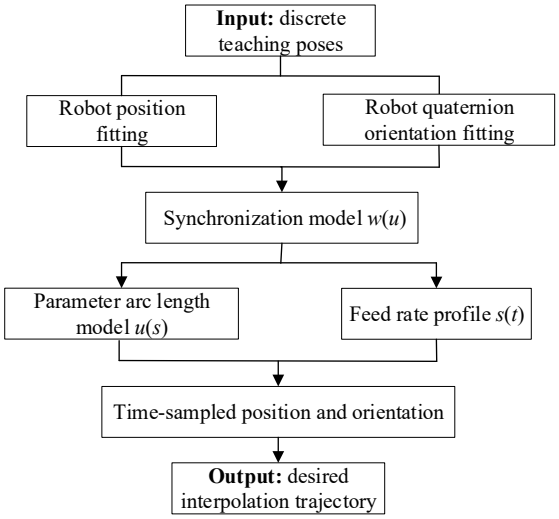

Figure 10. Flowchart of the trajectory planning method.

As shown in Figure 10, the positions and quaternion orientations are first fitted using the cubic B-spline curve $\boldsymbol{c}(u)$ and the quaternion spline curve $\boldsymbol{c}(w)$, respectively. Here, u and w are the geometric parameters. The position curve and the orientation curve must be synchronized before execution. Therefore, a parameter synchronization model $w(u)$ is

proposed to achieve smooth and synchronous motion of the robot. The robot path curve is described in $\mathbb{R}^7$ as follows:

$$\boldsymbol{C}(u) = \begin{Bmatrix} \boldsymbol{c}(u) \\ \widetilde{\boldsymbol{c}}(u) \end{Bmatrix} = \begin{Bmatrix} \boldsymbol{c}(u) \\ \boldsymbol{c}(w(u)) \end{Bmatrix} \tag{4}$$

Then, the learned feedrate profile, $s(t)$, and the u-s model, $u(s)$, are adopted to determine the motion law, $u(t)$, where s is the arc length parameter, t is the time parameter and $u(s)$ is a known function determined by the B-spline curve. Thus, the desired trajectory, $\widetilde{\boldsymbol{C}}(t) = \boldsymbol{C}(u(t))$, is determined.

Finally, the desired trajectory, $\widetilde{\boldsymbol{C}}(t)$, is discretized according to the system sampling period. Then, the discrete poses are converted into joint angles and the robot is controlled to move accordingly.

5. Impedance Control with Null-Space Optimization

This section proposes a computed-torque impedance control method for force tracking based on Ref. [25], as shown in Figure 11. Considering the safety of human–robot collaboration, the proposed impedance control method is implemented based on a 7-DOF collaborative robot. Therefore, null-space optimization also needs to be considered.

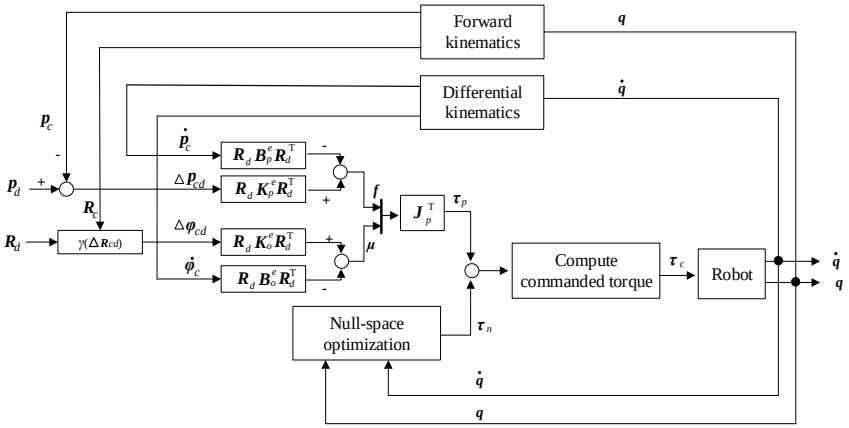

Figure 11. Impedance control with null-space optimization.

The impedance control parameters are designed at the robot end-effector and then transformed to the robot base coordinate system for execution. In addition, this method can achieve relatively accurate force skill transfer and surface finishing by integrating the desired trajectory and the desired force.

5.1. Dynamic Equation of Task Space

The dynamics of an n-link rigid robot in joint space is defined as follows:

$$\boldsymbol{H}(\boldsymbol{q})\ddot{\boldsymbol{q}} + \boldsymbol{C}(\boldsymbol{q}, \dot{\boldsymbol{q}}) + \boldsymbol{D}(\dot{\boldsymbol{q}}) + \boldsymbol{g}(\boldsymbol{q}) + \boldsymbol{\tau}_e = \boldsymbol{\tau}_c \tag{5}$$

where $\boldsymbol{H}(\boldsymbol{q}) \in \mathbb{R}^{n\times n}$ represents the inertial matrix. $\boldsymbol{C}(\boldsymbol{q}, \dot{\boldsymbol{q}}) \in \mathbb{R}^n$, $\boldsymbol{D}(\dot{\boldsymbol{q}}) \in \mathbb{R}^n$ and $\boldsymbol{g}(\boldsymbol{q}) \in \mathbb{R}^n$ represent the Coriolis, friction term and gravity term, respectively. $\boldsymbol{\tau}_c \in \mathbb{R}^n$ and $\boldsymbol{\tau}_e \in \mathbb{R}^n$ represent the actuator torque and the torque exerted by the robot on the environment, respectively.

For simplification, the following equations are introduced:

$$\begin{aligned} \boldsymbol{\tau}_c &= \boldsymbol{C}(\boldsymbol{q}, \dot{\boldsymbol{q}}) + \boldsymbol{D}(\dot{\boldsymbol{q}}) + \boldsymbol{g}(\boldsymbol{q}) + \boldsymbol{\tau}_e + \boldsymbol{\tau}_c' \\ \boldsymbol{H}(\boldsymbol{q})\ddot{\boldsymbol{q}} &= \boldsymbol{\tau}_c' \end{aligned} \tag{6}$$

Generally, the tasks performed by the robot are completed within the m-dimensional task space. Thus, it is more meaningful to design the controller in the task space than in the joint space. In addition, $\boldsymbol{\tau}_c' \in \mathbb{R}^n$ is the control variable. Therefore, the above equation in the task space can be represented as follows:

$$\begin{aligned} \boldsymbol{\Lambda}_p(\boldsymbol{q})\ddot{\boldsymbol{x}}_p - \boldsymbol{\Lambda}_p(\boldsymbol{q})\dot{\boldsymbol{J}}_p(\boldsymbol{q})\dot{\boldsymbol{q}} &= \boldsymbol{F}_p \\ \dot{\boldsymbol{x}}_p &= \boldsymbol{J}_p(\boldsymbol{q})\dot{\boldsymbol{q}} \\ \boldsymbol{\Lambda}_p(\boldsymbol{q}) &= (\boldsymbol{J}_p(\boldsymbol{q})\boldsymbol{H}^{-1}(\boldsymbol{q})\boldsymbol{J}_p^{\mathrm{T}}(\boldsymbol{q}))^{-1} \end{aligned} \tag{7}$$

where $\boldsymbol{\Lambda}_p(\boldsymbol{q}) \in \mathbb{R}^{m\times m}$ is the inertia matrix related to the task space; $\boldsymbol{J}_p(\boldsymbol{q}) \in \mathbb{R}^{m\times n}$ is the Jacobian matrix; $\boldsymbol{x}_p \in \mathbb{R}^m$ represent the pose in the task space; $\boldsymbol{\tau}_p \in \mathbb{R}^n$ and $\boldsymbol{F}_p \in \mathbb{R}^m$ represent the torque and force vectors related to $\boldsymbol{x}_p$, respectively.

5.2. Null-Space Optimization

For a redundant robot manipulator, there exists:

$$\boldsymbol{\tau}_c' = \boldsymbol{\tau}_p + \boldsymbol{\tau}_n \tag{8}$$

where $\boldsymbol{\tau}_p$ is used to complete the primary task. $\boldsymbol{\tau}_n$ is used to complete the secondary task, defined as follows:

$$\boldsymbol{\tau}_n = \boldsymbol{N}_p^{\mathrm{T}}(\boldsymbol{q})\boldsymbol{\tau}_s \tag{9}$$

$\boldsymbol{\tau}_n$ and $\boldsymbol{\tau}_p$ are decoupled. $\boldsymbol{\tau}_n$ is executed in the null space of $\boldsymbol{J}_p^{\mathrm{T}}(\boldsymbol{q})$, that is,

$$\boldsymbol{N}_p^{\mathrm{T}}(\boldsymbol{q}) = \left[\boldsymbol{I} - \bar{\boldsymbol{J}}_p(\boldsymbol{q})\boldsymbol{J}_p(\boldsymbol{q})\right]^{\mathrm{T}} = \left[\boldsymbol{I} - \boldsymbol{J}_p^{\mathrm{T}}(\boldsymbol{q})\bar{\boldsymbol{J}}_p^{\mathrm{T}}(\boldsymbol{q})\right] \tag{10}$$

where $\bar{\boldsymbol{J}}_p^{\mathrm{T}}(\boldsymbol{q}) \in \mathbb{R}^{m\times n}$ is the inverse of $\boldsymbol{J}_p(\boldsymbol{q})$, defined as follows:

$$\bar{\boldsymbol{J}}_p(\boldsymbol{q}) = \boldsymbol{H}^{-1}(\boldsymbol{q})\boldsymbol{J}_p^{\mathrm{T}}(\boldsymbol{q})\boldsymbol{\Lambda}_p(\boldsymbol{q}) \tag{11}$$

The robot pose is optimized by minimizing the gradients to keep the joints close to the mid-range values. Therefore, $\boldsymbol{\tau}_s$ is calculated as follows:

$$\boldsymbol{\tau}_s = \boldsymbol{H}(\boldsymbol{q})\boldsymbol{K}_N\frac{\partial \boldsymbol{v}(\boldsymbol{q})}{\partial \boldsymbol{q}} - \boldsymbol{K}_s\dot{\boldsymbol{q}} \tag{12}$$

where $\boldsymbol{K}_N/\boldsymbol{K}_s \in \mathbb{R}^{n\times n}$ is a diagonal gain matrix, and $\boldsymbol{K}_s = 2\sqrt{\boldsymbol{K}_N}$. $\boldsymbol{K}_s$ is used to avoid undesirable joint velocities. $\boldsymbol{v}(\boldsymbol{q})$ is a scalar equation, defined as follows:

$$\boldsymbol{v}(\boldsymbol{q}) = -\frac{1}{2}\sum_{i=1}^{n}\left(\frac{q_i - \bar{q}_i}{q_{i_M} - q_{i_m}}\right)^2 \tag{13}$$

where $\bar{q}_i$, q_{i_M} and q_{i_m} represent the middle, maximum and minimum values of the i-th joint, respectively.

5.3. Impedance Control

Impedance control is used to establish the dynamic relationship between the robot end-effector motion and the contact force, which can be expressed as follows:

$$\boldsymbol{M}\left(\ddot{\boldsymbol{x}}_p - \ddot{\boldsymbol{x}}_d\right) + \boldsymbol{B}\left(\dot{\boldsymbol{x}}_p - \dot{\boldsymbol{x}}_d\right) + \boldsymbol{K}\left(\boldsymbol{x}_p - \boldsymbol{x}_d\right) = \boldsymbol{F}_e \tag{14}$$

where $\boldsymbol{M}$, $\boldsymbol{B}$ and $\boldsymbol{K}$ represent the mass, damping and stiffness parameters, respectively. $\boldsymbol{x}_d$ represents the desired pose. $\boldsymbol{F}_e$ represents the force exerted by the end-effector on the environment.

In the task space, $\boldsymbol{F}_p$ represents the external force applied to the robot, which consists of the desired force, $\boldsymbol{F}_c$, and the environmental force, $\boldsymbol{F}_e$. Therefore, there exists:

$$\boldsymbol{F}_p = \boldsymbol{F}_c + \boldsymbol{F}_e \tag{15}$$

Let,

$$\boldsymbol{F}_c = -\boldsymbol{\Lambda}_p(\boldsymbol{q})\boldsymbol{j}_p(\boldsymbol{q})\dot{\boldsymbol{q}} + \widetilde{\boldsymbol{F}_p} \tag{16}$$

Then, the equation is obtained as follows:

$$\boldsymbol{\Lambda}_p(\boldsymbol{q})\ddot{\boldsymbol{x}}_p = \widetilde{\boldsymbol{F}_p} + \boldsymbol{F}_e \tag{17}$$

where $\widetilde{\boldsymbol{F}_p}$ is the new control variable, defined as follows:

$$\widetilde{\boldsymbol{F}_p} = \boldsymbol{\Lambda}_p(\boldsymbol{q})\ddot{\boldsymbol{x}}_p - \left[\boldsymbol{M}\left(\ddot{\boldsymbol{x}}_p - \ddot{\boldsymbol{x}}_d\right) + \boldsymbol{B}\left(\dot{\boldsymbol{x}}_p - \dot{\boldsymbol{x}}_d\right) + \boldsymbol{K}\left(\boldsymbol{x}_p - \boldsymbol{x}_d\right)\right] \tag{18}$$

To simplify the calculation, $\boldsymbol{M}$ is defined as follows:

$$\boldsymbol{M} = \left(\boldsymbol{J}_p(\boldsymbol{q})\boldsymbol{H}^{-1}(\boldsymbol{q})\boldsymbol{J}_p^{\mathrm{T}}(\boldsymbol{q})\right)^{-1} \tag{19}$$

Thus, Equation (18) is rewritten as follows:

$$\widetilde{\boldsymbol{F}_p} = \boldsymbol{\Lambda}_p(\boldsymbol{q})\ddot{\boldsymbol{x}}_d + \boldsymbol{B}\left(\dot{\boldsymbol{x}}_d - \dot{\boldsymbol{x}}_p\right) + \boldsymbol{K}\left(\boldsymbol{x}_d - \boldsymbol{x}_p\right) \tag{20}$$

Considering that $\ddot{\boldsymbol{x}}_d$ and $\dot{\boldsymbol{x}}_d$ are zero vectors, the above equation is simplified as follows:

$$\widetilde{\boldsymbol{F}_p} = -\boldsymbol{B}\dot{\boldsymbol{x}}_p + \boldsymbol{K}\left(\boldsymbol{x}_d - \boldsymbol{x}_p\right) \tag{21}$$

According to Ref. [25], $\boldsymbol{\tau}_p = \boldsymbol{J}_p^{\mathrm{T}}(\boldsymbol{q})\widetilde{\boldsymbol{F}_p} = \boldsymbol{J}_p^{\mathrm{T}}(\boldsymbol{q})\begin{bmatrix}\boldsymbol{f}\\ \boldsymbol{\mu}\end{bmatrix}$, where $\boldsymbol{f} \in \mathbb{R}^3$ and $\boldsymbol{\mu} \in \mathbb{R}^3$ represent force and torque, respectively.

$\boldsymbol{B}$ and $\boldsymbol{K}$ represent the damping and stiffness diagonal matrices relative to the robot base coordinate system, respectively. $\boldsymbol{B}_e$ and $\boldsymbol{K}_e$ represent the damping and stiffness diagonal matrices relative to the robot end-effector coordinate system, respectively. Thus, there exists:

$$\boldsymbol{B} = \boldsymbol{R}_d\boldsymbol{B}_e\boldsymbol{R}_d^{\mathrm{T}}, \boldsymbol{K} = \boldsymbol{R}_d\boldsymbol{K}_e\boldsymbol{R}_d^{\mathrm{T}} \tag{22}$$

where $\boldsymbol{R}_d$ is the rotation matrix of the robot end-effector relative to the robot base coordinate system.

The task space pose, $\boldsymbol{x}_p$, can be decomposed into position and orientation vectors as follows:

$$\boldsymbol{x}_p = \begin{bmatrix}\boldsymbol{p}_c\\ \boldsymbol{\varphi}_c\end{bmatrix} \tag{23}$$

where $\boldsymbol{p}_c \in \mathbb{R}^3$ represents the position, and $\boldsymbol{\varphi}_c \in \mathbb{R}^3$ represents the orientation. Thus, impedance control is used for position control and orientation control respectively.

(1) Position control

Assuming that $\boldsymbol{p}_c$ and $\boldsymbol{p}_d$ represent the current and desired positions of the end-effector relative to the robot base coordinate system, the force vector, $\boldsymbol{f}$, is calculated as follows:

$$\boldsymbol{f} = -\boldsymbol{B}_p\dot{\boldsymbol{p}}_c + \boldsymbol{K}_p\Delta\boldsymbol{p}_{cd} \tag{24}$$

where

$$\begin{aligned}\boldsymbol{B}_p &= \boldsymbol{R}_d\boldsymbol{B}_p^e\boldsymbol{R}_d^{\mathrm{T}}\\ \boldsymbol{K}_p &= \boldsymbol{R}_d\boldsymbol{K}_p^e\boldsymbol{R}_d^{\mathrm{T}}\end{aligned} \tag{25}$$

where $\boldsymbol{B}_p^e \in \mathbb{R}^{3\times3}$ and $\boldsymbol{K}_p^e \in \mathbb{R}^{3\times3}$ are the damping and stiffness diagonal matrices of the position, respectively.

Furthermore, the position error, $\Delta\boldsymbol{p}_{cd}$, is calculated as follows:

$$\Delta\boldsymbol{p}_{cd}[k] = \boldsymbol{p}_d[k] - \boldsymbol{p}_c[k] \tag{26}$$

where k represents the iteration number of the control system.

(2) Orientation control

The rotational error is calculated as follows:

$$\Delta\boldsymbol{R}_{cd} = \boldsymbol{R}_d\boldsymbol{R}_c^{-1} \tag{27}$$

where $\boldsymbol{R}_c$ and $\boldsymbol{R}_d$ represent the current and desired rotation matrices of the end-effector, respectively.

To avoid singularity issues, the rotational vector is defined as follows:

$$\gamma(\boldsymbol{R}) = \frac{1}{2}\begin{bmatrix} r_{32} - r_{23} \\ r_{13} - r_{31} \\ r_{21} - r_{12} \end{bmatrix} \tag{28}$$

Thus, the orientation error is given by:

$$\Delta\boldsymbol{\varphi}_{cd} = \gamma(\Delta\boldsymbol{R}_{cd}) \tag{29}$$

The torque vector, $\boldsymbol{\mu}$, is calculated as follows:

$$\boldsymbol{\mu} = -\boldsymbol{B}_o\dot{\boldsymbol{\varphi}}_c + \boldsymbol{K}_o\Delta\boldsymbol{\varphi}_{cd} \tag{30}$$

where

$$\begin{aligned} \boldsymbol{B}_o &= \boldsymbol{R}_d\boldsymbol{B}_o^e\boldsymbol{R}_d^{\mathrm{T}} \\ \boldsymbol{K}_o &= \boldsymbol{R}_d\boldsymbol{K}_o^e\boldsymbol{R}_d^{\mathrm{T}} \end{aligned} \tag{31}$$

where $\boldsymbol{B}_o^e \in \mathbb{R}^{3\times3}$ and $\boldsymbol{K}_o^e \in \mathbb{R}^{3\times3}$ are the damping and stiffness diagonal matrices of the orientation, respectively.

Furthermore, the position velocity $\dot{\boldsymbol{p}}_c$ and angular velocity $\dot{\boldsymbol{\varphi}}_c$ are calculated as follows:

$$\begin{bmatrix} \dot{\boldsymbol{p}}_c \\ \dot{\boldsymbol{\varphi}}_c \end{bmatrix} = \boldsymbol{J}_p(\boldsymbol{q})\dot{\boldsymbol{q}} \tag{32}$$

Finally, the command torque, $\boldsymbol{\tau}_c$, is obtained as follows:

$$\boldsymbol{\tau}_c = \boldsymbol{J}_p^{\mathrm{T}}(\boldsymbol{q})\widetilde{\boldsymbol{F}}_p + \boldsymbol{N}_p^{\mathrm{T}}(\boldsymbol{q})\boldsymbol{\tau}_s + \boldsymbol{C}(\boldsymbol{q},\dot{\boldsymbol{q}})\dot{\boldsymbol{q}} + \boldsymbol{g}(\boldsymbol{q}) + \boldsymbol{J}_p^{\mathrm{T}}(\boldsymbol{q})\hat{\boldsymbol{F}}_e \tag{33}$$

where $\hat{\boldsymbol{F}}_e = \begin{bmatrix} 0 & 0 & F_z & 0 & 0 & 0 \end{bmatrix}^{\mathrm{T}}$. F_z represents the learned desired force. In addition, the friction term $\boldsymbol{D}(\dot{\boldsymbol{q}})$ is neglected.

6. Experiment

To verify the effectiveness of the proposed force control method, the experiment is carried out on the platform shown in Figure 12. The platform consists of a 7-DOF robot manipulator from Franka Emika, a handheld pneumatic sanding tool, an air pump and a complex violin surface. The robot control cycle is 1 ms, and each joint is equipped with a joint torque sensor to sense the external contact force.

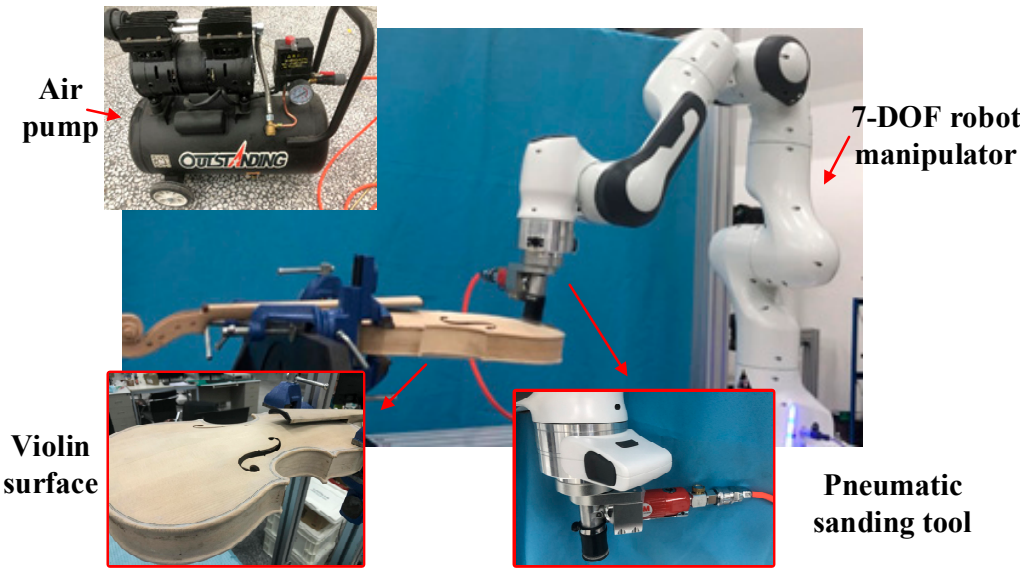

Figure 12. Experimental platform for human-robot assisted sanding.

The experiment is mainly divided into the following two steps: (1) generating a continuous desired trajectory based on discrete teaching poses and (2) relatively accurate force skill transfer and sanding of the complex surface.

(1) Generate a continuous desired trajectory

Firstly, the user grasps the pneumatic sanding tool under gravity compensation to teach the discrete poses on the violin surface. Then, the learned feedrate profile is combined with the trajectory planning algorithm in Section 4 to generate the continuous desired trajectory, as shown in Figure 13.

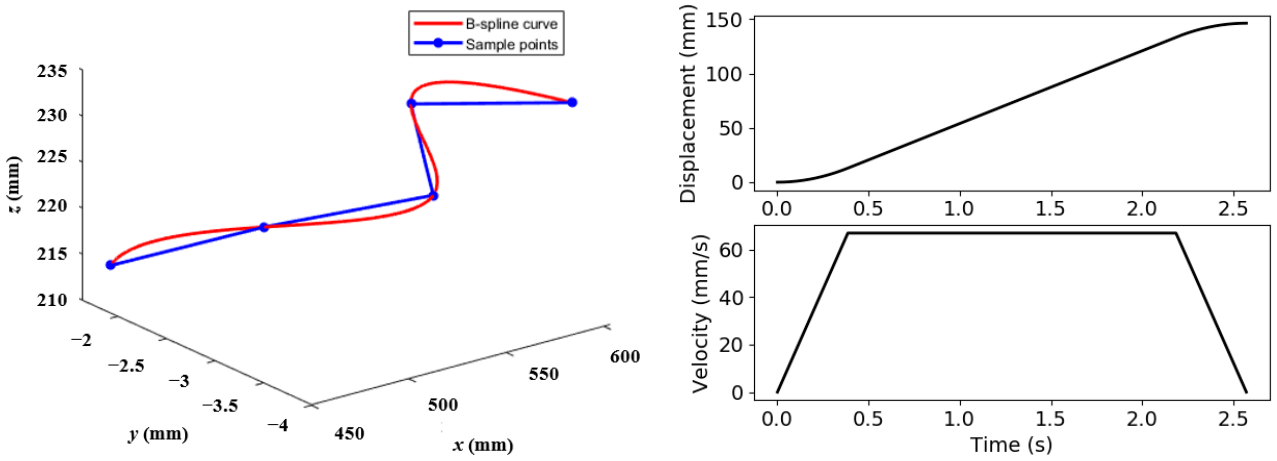

Figure 13. The desired trajectory generated based on discrete teaching poses: (**a**) generated path curve; (**b**) T-shaped feedrate profile.

The desired trajectory, $\widetilde{\boldsymbol{C}}(t)$, consists of the path curve, $\boldsymbol{C}(u)$, and the motion law $u(t)$. $u(t)$ is determined by $u(s)$ and the learned T-shaped feedrate profile $s(t)$. $u(s)$ is a known function determined by the B-spline curve. The feedrate planning of the trajectory is based on the arc length of the path curve, v_{max} and a_{max}.

The feedrate profile of the sanding trajectory is shown in Figure 13b. Firstly, the robot accelerates uniformly at the maximum acceleration until it reaches the maximum velocity. Then, the uniform motion is maintained. Finally, the robot decelerates uniformly at the

maximum acceleration. In addition, the initial and final velocities of the robot are both zero, ensuring the smoothness of the entire motion process.

(2) Force skill transfer and violin surface sanding

To verify the performance of the proposed force control method, an actual sanding experiment is conducted. During sanding, the robot moves back and forth along the desired trajectory. The controller parameters are selected through extensive testing to obtain good performance, as shown in Table 1.

Table 1. Impedance control parameters and null-space gain.

Control Object	Parameter Value
Position	$\boldsymbol{B}_p^e = \begin{bmatrix} 30 & 0 & 0 \\ 0 & 30 & 0 \\ 0 & 0 & 100 \end{bmatrix}, \boldsymbol{K}_p^e = \begin{bmatrix} 1500 & 0 & 0 \\ 0 & 1500 & 0 \\ 0 & 0 & 100 \end{bmatrix}$
Orientation	$\boldsymbol{B}_o^e = \begin{bmatrix} 10 & 0 & 0 \\ 0 & 10 & 0 \\ 0 & 0 & 10 \end{bmatrix}, K_o^e = \begin{bmatrix} 200 & 0 & 0 \\ 0 & 200 & 0 \\ 0 & 0 & 200 \end{bmatrix}$
Null-space gain	$\boldsymbol{K}_N \in \mathbb{R}^{7\times 7} = \begin{bmatrix} 200 & \cdots & 0 \\ \vdots & \ddots & \vdots \\ 0 & \cdots & 200 \end{bmatrix}$

Then, the force tracking data during sanding are recoded. The recorded force data, excluding the sensor zero-drift values, are shown in Figure 14.

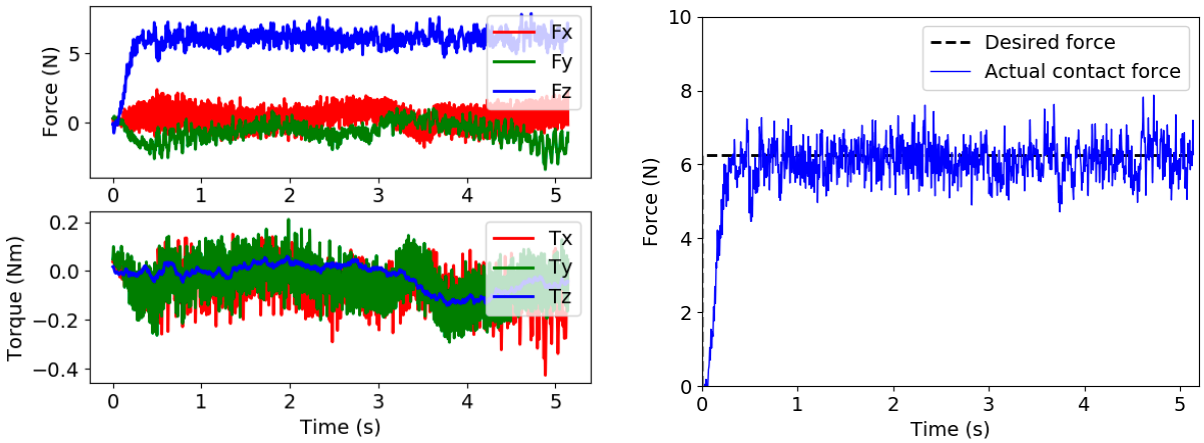

(**a**) (**b**)

Figure 14. The transferred force skill: (**a**) force/torque values; (**b**) normal sanding force.

It can be seen from Figures 4 and 14 that the force/torque values are similar. Thus, it can be concluded that the proposed force control method can relatively accurately realize the learning and transfer of force skills. Furthermore, this method can achieve the sanding of the complex violin surface. The surface quality before and after sanding is shown in Figure 15. The results show that the surface is smoother and brighter after sanding.

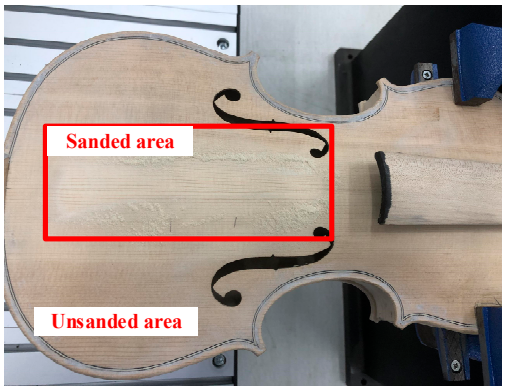

Figure 15. Comparison of the violin surface before and after sanding.

In summary, the proposed force control method can achieve relatively accurate force skill transfer and sanding of complex surfaces, thereby improving the surface quality of the workpiece.

7. Conclusions

This paper proposes a force control method that incorporates human skills to achieve relatively accurate force skill transfer and complex surface finishing. The method mainly consists of three parts: (1) human skills learning, (2) continuous desired trajectory generation and (3) a computed-torque impedance control method. Furthermore, the proposed force control method is introduced by taking the sanding of a complex wooden surface as an example. The advantages of the proposed method are summarized as follows:

(1) Human skills are deeply analyzed and decomposed into motion skill and force skill. Thus, these human skills are easy to learn and transfer.
(2) A robot trajectory planning method based on spline curves is provided to generate the desired trajectory, meeting the requirements of complex surface trajectory planning.
(3) A computed-torque impedance control architecture considering null-space optimization is proposed. By incorporating the desired trajectory and the desired force, constant force tracking is achieved.
(4) The experiments demonstrate that the proposed force control method can achieve relatively accurate force skill transfer and improve the surface quality of the workpiece.

Author Contributions: Conceptualization, K.M.; methodology, K.M.; software, K.M.; validation, K.M.; resources, F.N. and H.L.; writing—original draft preparation, K.M.; writing—review and editing, F.N. and Z.C.; supervision, H.L.; project administration, F.N.; funding acquisition, F.N. All authors have read and agreed to the published version of the manuscript.

Funding: This research was funded by the National Natural Science Foundation of China (grant number: 51875114) and the Self-Planned Task (grant number: SKLRS202204B) of the State Key Laboratory of Robotics and System (HIT).

Institutional Review Board Statement: Not applicable.

Data Availability Statement: Data are contained within the article.

Conflicts of Interest: The authors declare no conflicts of interest.

References

1. Schneyer, S.; Sachtler, A.; Eiband, T.; Nottensteiner, K. Segmentation and coverage planning of freeform geometries for robotic surface finishing. *IEEE Robot. Autom. Lett.* **2023**, *8*, 5267–5274. [CrossRef]
2. Zhu, D.H.; Feng, X.Z.; Xu, X.H.; Yang, Z.Y.; Li, W.L.; Yan, S.J.; Ding, H. Robotic grinding of complex components: A step towards efficient and intelligent machining-challenges, solutions, and applications. *Robot. Comput.-Integr. Manuf.* **2020**, *65*, 101908. [CrossRef]

3. Yang, Z.Y.; Chu, Y.; Xu, X.H.; Huang, H.J.; Zhu, D.H.; Yan, S.J.; Ding, H. Prediction and analysis of material removal characteristics for robotic belt grinding based on single spherical abrasive grain model. *Int. J. Mech. Sci.* **2021**, *190*, 106005. [CrossRef]
4. Li, W.L.; Xie, H.; Zhang, G.; Yan, S.J.; Yin, Z.P. Hand-eye calibration in visually-guided robot grinding. *IEEE Trans. Cybern.* **2016**, *46*, 2634–2642. [CrossRef] [PubMed]
5. Perez-Vidal, C.; Gracia, L.; Sanchez-Caballero, S.; Solanes, J.E.; Saccon, A.; Tornero, J. Design of a polishing tool for collaborative robotics using minimum viable product approach. *Int. J. Comput. Integr. Manuf.* **2019**, *32*, 848–857. [CrossRef]
6. Wahballa, H.; Duan, J.J.; Dai, Z.D. An automatic robot polishing control method for compound surface comprising plane and curved surfaces. *Int. J. Adv. Manuf. Technol.* **2024**, *132*, 3801–3819. [CrossRef]
7. Nguyen, J.; Bailey, M.; Carlucho, I.; Barbalata, C. Robotic manipulators performing smart sanding operation: A vibration approach. In Proceedings of the IEEE International Conference on Robotics and Automation (ICRA), Philadelphia, PA, USA, 23–27 May 2022; pp. 2958–2964.
8. Nagata, F.; Kusumoto, Y.; Fujimoto, Y.; Watanabe, K. Robotic sanding system for new designed furniture with free-formed surface. *Robot. Comput.-Integr. Manuf.* **2007**, *23*, 371–379. [CrossRef]
9. Huo, Y.X.; Li, P.; Chen, D.C.; Liu, Y.H.; Li, X. Model-free adaptive impedance control for autonomous robotic sanding. *IEEE Trans. Autom. Sci. Eng.* **2022**, *19*, 3601–3611. [CrossRef]
10. Zhang, B.X.; Wu, S.J.; Wang, D.Z.; Yang, S.L.; Jiang, F.; Li, C.H. A review of surface quality control technology for robotic abrasive belt grinding of aero-engine blades. *Measurement* **2023**, *220*, 113381. [CrossRef]
11. Ma, K.W.; Han, L.; Sun, X.X.; Liang, C.; Zhang, S.S.; Shi, Y.D.; Wang, X.S. A path planning method of robotic belt grinding for workpieces with complex surfaces. *IEEE/ASME Trans. Mechatron.* **2020**, *25*, 728–738. [CrossRef]
12. Xiao, M.B.; Ding, Y.; Yang, G.L. A model-based trajectory planning method for robotic polishing of complex surfaces. *IEEE Trans. Autom. Sci. Eng.* **2022**, *19*, 2890–2903. [CrossRef]
13. Zhou, P.; Zhao, X.W.; Tao, B.; Ding, H. Combination of dynamical movement primitives with trajectory segmentation and node mapping for robot machining motion learning. *IEEE/ASME Trans. Mechatron.* **2023**, *28*, 175–185. [CrossRef]
14. Wang, Z.L.; Zou, L.; Duan, L.; Liu, X.F.; Lv, C.; Gong, M.W.; Huang, Y. Study on passive compliance control in robotic belt grinding of nickel-based superalloy blade. *J. Manuf. Process.* **2021**, *68*, 168–179. [CrossRef]
15. Chen, H.Q.; Yang, J.X.; Ding, H. Robotic compliant grinding of curved parts based on a designed active force-controlled end-effector with optimized series elastic component. *Robot. Comput.-Integr. Manuf.* **2024**, *86*, 102646. [CrossRef]
16. Zhang, H.Y.; Li, L.; Zhao, J.B.; Zhao, J.C.; Liu, S.J.; Wu, J.J. Design and implementation of hybrid force/position control for robot automation grinding aviation blade based on fuzzy PID. *Int. J. Adv. Manuf. Technol.* **2020**, *107*, 1741–1754. [CrossRef]
17. Han, F.T.; Tam, S.Y.; Cao, Z.H.; Zhao, X.W.; Tao, B.; Ding, H. Nonlinear impedance control with trajectory adaptation for collaborative robotic grinding. *Sci. China-Technol. Sci.* **2023**, *66*, 1928–1936. [CrossRef]
18. Du, G.L.; Chen, M.X.; Liu, C.B.; Zhang, B.; Zhang, P. Online robot teaching with natural human-robot interaction. *IEEE Trans. Ind. Electron.* **2018**, *65*, 9571–9581. [CrossRef]
19. Xie, H.L.; Wang, Q.H.; Ong, S.K.; Li, J.R.; Chi, Z.P. Adaptive human-robot collaboration for robotic grinding of complex workpieces. *CIRP Ann.* **2022**, *71*, 285–288. [CrossRef]
20. Ng, C.W.X.; Chan, K.H.K.; Teo, W.K.; Chen, I.M. A method for capturing the tacit knowledge in the surface finishing skill by demonstration for programming a robot. In Proceedings of the IEEE International Conference on Robotics and Automation (ICRA), Hong Kong, China, 31 May–7 June 2014; pp. 1374–1379.
21. Ng, W.X.; Chan, H.K.; Teo, W.K.; Chen, I.M. Programming a robot for conformance grinding of complex shapes by capturing the tacit knowledge of a skilled operator. *IEEE Trans. Autom. Sci. Eng.* **2017**, *14*, 1020–1030. [CrossRef]
22. Ng, W.X.; Chan, H.K.; Teo, W.K.; Chen, I.M. Capturing the tacit knowledge of the skilled operator to program tool paths and tool orientations for robot belt grinding. *Int. J. Adv. Manuf. Technol.* **2017**, *91*, 1599–1618. [CrossRef]
23. Gao, X.; Ling, J.; Xiao, X.H.; Li, M. Learning force-relevant skills from human demonstration. *Complexity* **2019**, 5262859. [CrossRef]
24. Zhang, G.J.; Ni, F.L.; Liu, H.; Jiang, Z.N.; Yang, G.C.; Li, C.Y. Learning impedance regulation skills for robot belt grinding from human demonstrations. *Assem. Autom.* **2021**, *41*, 431–440.
25. Ochoa, H.; Cortesão, R. Impedance control architecture for robotic-assisted mold polishing based on human demonstration. *IEEE Trans. Ind. Electron.* **2021**, *69*, 3822–3830. [CrossRef]
26. Ochoa, H.; Cortesão, R. Control architecture for robotic-assisted polishing tasks based on human skills. In Proceedings of the 45th Annual Conference of the IEEE Industrial Electronics Society (IECON), Lisbon, Portugal, 14–17 October 2019; pp. 630–637.
27. Min, K.; Ni, F.L.; Zhang, G.J.; Shu, X.; Liu, H. A C2 continuous trajectory planning method for 6-DOF rotational robot manipulators. *Assem. Autom.* **2022**, *42*, 616–627. [CrossRef]

Disclaimer/Publisher's Note: The statements, opinions and data contained in all publications are solely those of the individual author(s) and contributor(s) and not of MDPI and/or the editor(s). MDPI and/or the editor(s) disclaim responsibility for any injury to people or property resulting from any ideas, methods, instructions or products referred to in the content.